Available online at www.sciencedirect.com
ScienceDirect
Composites: Part A 37 (2006) 1722–1733
composites
Part A: applied science and manufacturing
www.elsevier.com/locate/compositesa

Modelling of fatigue crack tunneling and delamination in layered composites

Akke S.J. Suiker [a,*], Norman A. Fleck [b]

[a] Delft University of Technology, Koiter Institute Delft/Faculty of Aerospace Engineering, P.O. Box 5058, 2600 GB Delft, The Netherlands
[b] Cambridge University, Cambridge Centre for Micromechanics, Department of Engineering, Trumpington Street, Cambridge, CB2 1PZ, United Kingdom

Received 28 February 2005; received in revised form 16 September 2005; accepted 17 September 2005

Abstract

A review of the literature reveals that fatigue cracks in layered composites may grow at a constant rate in a steady-state configuration. Cracks can tunnel as mode I cracks in a constrained layer, with or without delamination of adjacent plies. Alternatively, progressive plane-strain delamination may occur from the ends of a plane-strain mode I crack. In the present paper the relationship between fatigue crack growth rate and remote cyclic stress is predicted for steady-state tunneling cracks and for plane-strain delaminating cracks. The fatigue models make use of Paris-type crack growth laws. The predictions for plane-strain delamination are in excellent agreement with existing experimental data for fatigue delamination growth in fibre–metal laminates.

Keywords: A. Fibres; A. Laminates; B. Fracture; B. Stress concentrations

1. Introduction

The fatigue damage tolerance of laminated solids, such as fibre-reinforced composites and fibre–metal laminates, is often achieved through the mechanism of crack deflection. The use of brittle interfaces between fibres and matrix, or between individual layers of a laminate, can induce crack deflection along the interface, thereby protecting the structure against failure on a single mode I plane [1–19]. For example, tunneling of an H-shape crack, see Fig. 1, has been observed in the fatigue cracking of 0/90 cross-ply carbon fibre–epoxy matrix laminates, and in fibre–metal laminates such as ARALL and GLARE[1], see for example [1,12,15]. The sequence of crack development to form a tunneling H-shaped fatigue crack is as follows. Assume an initial defect approximating that of a penny shaped crack within a metal layer of the fibre–metal laminates. Under cyclic loading an elliptical fatigue crack develops from this flaw and grows within the sandwiched metal layer. The crack reaches the adjacent fibre–epoxy layers, and kinks into a pair of opposing delamination cracks. Fatigue crack crack growth along the delaminations gives the crack an H-shape. When the interface is resistant to continued fatigue crack growth, the delaminations may arrest and tunneling of the H-shape crack then ensures.

In this paper, three competing mechanisms of fatigue crack growth are addressed for alternating layers of two dissimilar but isotropic elastic solids, indicated as materials "1" and "2" in Fig. 2. The mechanisms are (i) tunneling of a purely mode I crack in a material 1 layer (*mechanism 1*), (ii) tunneling of an H-shape crack, with delaminations of constant length l (*mechanism 2*), and (iii) tunneling of an H-shape crack with continuously growing delamination (*mechanism 3*). It will be demonstrated that the selection of a specific mechanism depends upon the value of the

* Corresponding author. Tel.: +31 15 2781629; fax: +31 15 2611465.
E-mail addresses: A.Suiker@lr.tudelft.nl (A.S.J. Suiker), Naf1@eng.cam.ac.uk (N.A. Fleck).

[1] ARALL and GLARE are laminates consisting of an alternating stack of aluminium alloy sheets and fibre–epoxy layers. ARALL laminates are reinforced by aramid fibres and GLARE laminates are reinforced by glass fibres. An overview of the manufacturing, characteristic properties and applications of these laminates can be found in [15].

1359-835X/$ - see front matter © 2005 Elsevier Ltd. All rights reserved.
doi:10.1016/j.compositesa.2005.09.006

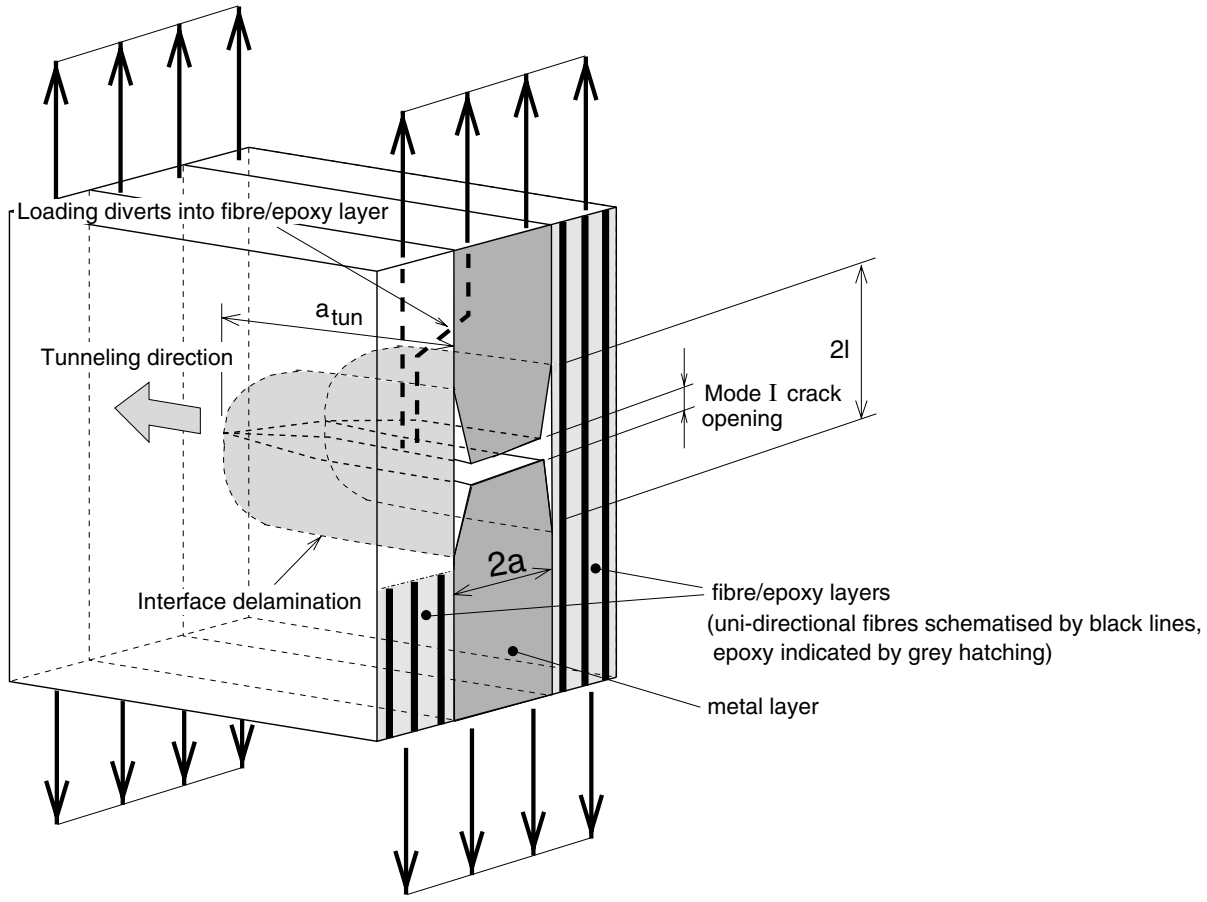

Fig. 1. H-shape crack tunneling in a fibre–metal laminate.

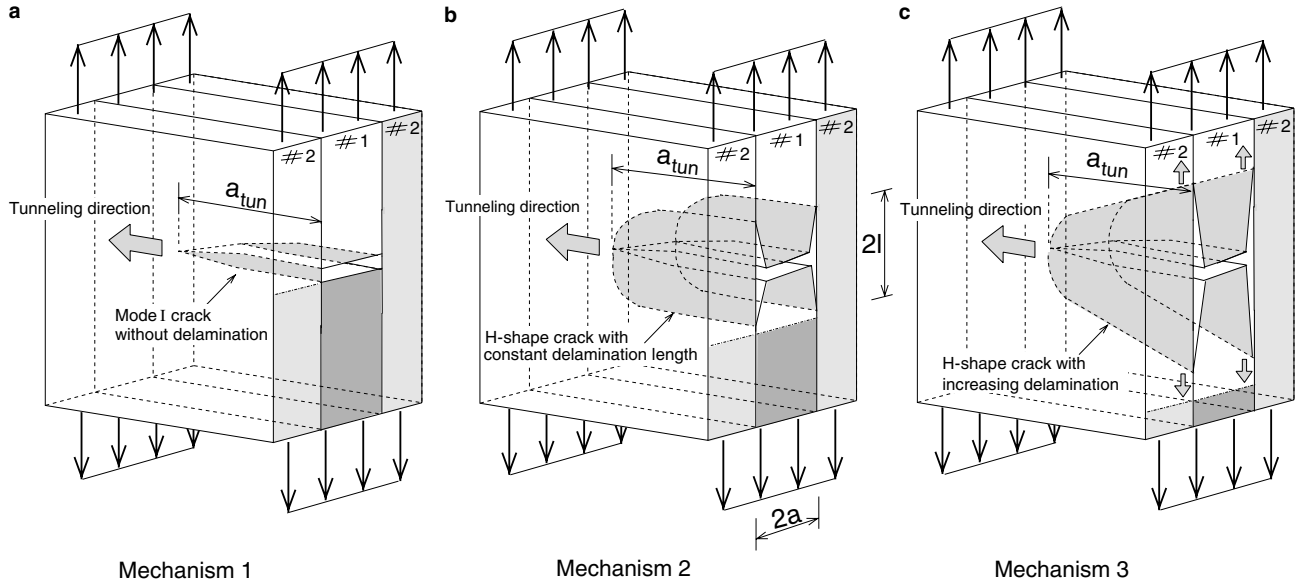

Fig. 2. Three possible failure mechanisms for a laminate of two dissimilar, isotropic materials. *Mechanism 1*: Tunneling of a mode I crack without delamination. *Mechanism 2*: Tunneling of an H-shape crack with constant delamination. *Mechanism 3*: Tunneling of an H-shape crack with continuously increasing delamination.

cyclic mode I stress intensity factor at the tunneling crack front, the fatigue threshold stress intensity factor for delamination, and the stiffness mismatch between the layers. The assumption of elastic isotropic layers may be acceptable for laminates with fibres in multiple directions, where the elastic mismatch between the fibres and the

surrounding matrix is moderate. A detailed study of the above mechanisms under monotonic loading can be found in Suiker and Fleck [20].

The main aim is to develop fatigue models for the above crack tunneling and delamination mechanisms, in which the growth rate is expressed in terms of the magnitude of the applied cyclic loading. The models require the determination of specific functions that account for the fracture geometry analysed. These functions can be obtained numerically through 2D finite element analyses, see Suiker and Fleck [20]. In these analyses it is assumed that initial defects are sufficiently large for the nucleation phase of cracking to be irrelevant, and a tunneling crack is supposed to have reached a steady state, i.e. the tunneling front has a constant shape, and the delamination length is fixed. The remote stress for a 3D steady-state tunneling crack can then be derived from a plane-strain elasticity solution, through equating the strain energy difference upstream and downstream of the tunneling front to the energy released per tunneling depth. In the present paper results from the numerical study of Suiker and Fleck [20] are reduced to fatigue fracture maps. After the Paris-type fatigue law has been specified, the tunneling mechanism and crack growth rate can be determined as a function of the level of cyclic stress. In addition, an analytical model is derived for the determination of the growth rate of a continuously lengthening, plane-strain H-shape crack reaching the limit of infinitely large delamination. The ability of this model to accurately predict delamination growth rates is demonstrated by means of a comparison with experimental fatigue data for ARALL laminates, as reported by Marissen [1].

2. Analysis of fatigue mechanisms

For laminates subjected to remote tensile fatigue loading, the crack growth rates related to the tunneling mechanisms sketched in Fig. 2 are assumed to be governed by the cyclic stress intensity factor ΔK_{I} of the mode I crack in the material 1 layer. This stress intensity factor is given by,

$$\Delta K_{\mathrm{I}} = K_{\mathrm{I,max}} - K_{\mathrm{I,min}}, \tag{1}$$

where $K_{\mathrm{I,max}}$ and $K_{\mathrm{I,min}}$ are the maximum and minimum mode I stress intensity factors during a fatigue cycle. The crack growth rate $\mathrm{d}a_{\mathrm{tun}}/\mathrm{d}N$ for these crack geometries may be computed by the usual Paris relation [21],

$$\frac{\mathrm{d}a_{\mathrm{tun}}}{\mathrm{d}N} = A(\Delta K_{\mathrm{I}})^p, \tag{2}$$

where A and p are material constants, with the exponent p typically in the range of 2–8 for metals.

For a delaminating crack propagating along a bi-material interface, the delamination stress intensity factor K_{d} is given by

$$K_{\mathrm{d}} r^{i\varepsilon} = K_{\mathrm{d,I}} + iK_{\mathrm{d,II}}, \tag{3}$$

where $K_{\mathrm{d,I}}$ and $K_{\mathrm{d,II}}$ are the mode I and mode II components of the delamination stress intensity factor and $i = \sqrt{-1}$. Further, $r^{i\varepsilon}$ is the oscillatory term, which is characterised by the oscillatory index ε, and the distance r directly ahead of the crack tip [22,23]. The magnitude of the delamination stress intensity factor is

$$|K_{\mathrm{d}}| = \sqrt{K_{\mathrm{d,1}}^2 + K_{\mathrm{d,2}}^2}. \tag{4}$$

Analogous to Eq. (1), the cyclic stress intensity factor of the delaminating crack may be expressed as

$$\Delta K_{\mathrm{d}} = |K_{\mathrm{d}}|_{\mathrm{max}} - |K_{\mathrm{d}}|_{\mathrm{min}}, \tag{5}$$

where $|K_{\mathrm{d}}|_{\mathrm{max}}$ and $|K_{\mathrm{d}}|_{\mathrm{min}}$ are the maximum and minimum values of the delamination stress intensity factor during a fatigue cycle. The delamination growth rate, $\mathrm{d}l/\mathrm{d}N$, at the interface between the material 1 and material 2 layers is supposed to follow a relation similar to Eq. (2), i.e.

$$\frac{\mathrm{d}l}{\mathrm{d}N} = B(\Delta K_{\mathrm{d}})^s, \tag{6}$$

where B and s are material constants. It is expected that these material constants will depend upon the mode-mixity of the interface delamination. However, the study of Suiker and Fleck [20] showed that the mode-mixity usually attains a steady-state value at relatively small delamination lengths; hence the assumption of a constant mode-mixity does not introduce large errors.

In order to establish relations between the crack growth rates $\mathrm{d}a_{\mathrm{tun}}/\mathrm{d}N$, $\mathrm{d}l/\mathrm{d}N$, and the amplitude of the remote fatigue loading $\Delta\sigma_1$, the stress intensity factors ΔK_{I} and ΔK_{d} in Eqs. (2) and (6) need to be expressed in terms of $\Delta\sigma_1$. This is done below by considering in turn the *mechanisms 1*, *2*, and *3* of Fig. 2 for a load ratio $R = K_{\mathrm{min}}/K_{\mathrm{max}}$ equal to zero. Accordingly, the cyclic stress intensity factors Eqs. (1) and (5), respectively, reduce to

$$\Delta K_{\mathrm{I}} = K_{\mathrm{I,max}}, \qquad \Delta K_{\mathrm{d}} = |K_{\mathrm{d}}|_{\mathrm{max}}. \tag{7}$$

2.1. Mechanism 1

As sketched in Fig. 2a, *mechanism 1* corresponds to the fatigue tunneling of a mode I crack in one layer of material 1, and absent delamination at the interfaces with the adjacent uncracked plies. The width of the mode I crack is $2a$ and is equal to the thickness of the material 1 layer. The applied loading comprises a remote cyclic strain $\Delta\varepsilon$, which corresponds to cyclic stresses of magnitudes $\Delta\sigma_1$ and $\Delta\sigma_2$ in the material 1 and 2 layers, respectively. By strain compatibility across the coherent interface between the layers, these cyclic stresses are related to each other as $\Delta\sigma_1 = \Delta\sigma_2\bar{E}_1/\bar{E}_2$. The overbar on the Young's modulus denotes the plane–strain value, $\bar{E}_i \equiv E/(1-\nu_i^2)$, with ν_i the Poisson's ratio and $i \in 1, 2$. The procedure to establish a relation between $\Delta\sigma_1$ and the fatigue crack growth rate of the tunneling crack, $\mathrm{d}a_{\mathrm{tun}}/\mathrm{d}N$, uses the general framework presented in Suiker and Fleck [20], and only the main steps are summarised below.

Consider first a mode I crack growing under *monotonic loading* (remotely σ_1 in the layer of material 1 and σ_2 in the

layer of material 2). When the crack tunnels in steady state, the tunneling front has a constant shape and the energy release rate is independent of the length of the tunneling crack. The energy released per unit tunneling depth can be computed as the difference in elastic strain energy ΔW downstream and upstream of the tunneling front [24–26,20],

$$\Delta W = \frac{1}{2}\sigma_1 \bar{\delta} 2a, \tag{8}$$

where $\bar{\delta}$ equals the average displacement over the mode I crack faces. By dimensional considerations, $\bar{\delta}$ can be written in the form

$$\bar{\delta} = \frac{a\sigma_1}{\bar{E}_1} f(\bar{E}_2/\bar{E}_1), \tag{9}$$

where the dimensionless function f depends upon the stiffness ratio $\bar{E}_2/\bar{E}_1$. Now introduce the mode I energy release rate G_I per unit area of tunnel crack surface. Combining the energy balance

$$\Delta W = 2aG_I \tag{10}$$

with Eqs. (8) and (9) leads to

$$\sigma_1 = K_I \sqrt{\frac{2}{af(\bar{E}_2/\bar{E}_1)}}, \tag{11}$$

where K_I is related to G_I by the usual Irwin relation,

$$K_I = \sqrt{G_I \bar{E}_1}. \tag{12}$$

Upon equating K_I with the mode I fracture toughness of material 1, K_{Ic}, Eq. (11) gives the magnitude of the tunneling stress for the mode I crack. Instead, invert Eq. (11) to obtain

$$K_I = \sigma_1 \sqrt{\frac{a}{2} f(\bar{E}_2/\bar{E}_1)}. \tag{13}$$

This relation gives the tunneling stress intensity factor for an applied remote stress σ_1. For the case of fatigue loading with amplitude $\Delta\sigma_1$, the corresponding cyclic mode I stress intensity factor is

$$\Delta K_I = \Delta\sigma_1 \sqrt{\frac{a}{2} f(\bar{E}_2/\bar{E}_1)}. \tag{14}$$

Substitution of this relation into the Paris law, Eq. (2), gives the predicted tunneling crack growth rate, da_{tun}/dN.

2.2. Mechanism 2

Second, consider a tunneling H-shape crack with constant delaminations l, as depicted in Fig. 2b. The theory is developed first for monotonic loading, and then modified for cyclic loading. The energy released per unit tunneling depth can be expressed as:

$$\Delta W = 2aG_I + 4lG_d, \tag{15}$$

where G_d is the delamination energy release rate and G_I is the mode I energy release rate during tunneling. Equating the above expression with Eq. (8) leads to

$$\sigma_1 \bar{\delta} a = 2aG_I + 4lG_d. \tag{16}$$

The average displacement over the mode I crack faces is now expressed by

$$\bar{\delta} = \frac{a\sigma_1}{\bar{E}_1} g(l/a, \bar{E}_2/\bar{E}_1), \tag{17}$$

with the dimensionless function g depending upon the aspect ratio of the H-shape crack l/a and upon the stiffness ratio $\bar{E}_2/\bar{E}_1$. Eqs. (16) and (17) can be rephrased in terms of delamination stress intensity factor K_d using the form

$$|K_d| = \sqrt{G_d E_* \cosh^2(\pi\varepsilon)}. \tag{18}$$

Here E_* is a combined stiffness parameter given by $E_* = 2(\bar{E}_1^{-1} + \bar{E}_2^{-1})^{-1}$, and ε is the oscillatory index

$$\varepsilon = \frac{1}{2\pi} \ln\left(\frac{1-\beta}{1+\beta}\right) \tag{19}$$

in terms of the Dundur's parameter β [27], where

$$\beta = \frac{1}{2}\frac{(1-2\nu_2)/\mu_2 - (1-2\nu_1)/\mu_1}{(1-\nu_2)/\mu_2 + (1-\nu_1)/\mu_1}. \tag{20}$$

The Dundur's parameter β is prescribed by the Poisson's ratio ν_i and the shear modulus $\mu_i = E_i/2(1+\nu_i)$ of the materials $i \in 1, 2$. Combining Eqs. (12), (16), (17) and (18) results in

$$\sigma_1 = \left(\frac{2aK_I^2}{\bar{E}_1} + \frac{4l\,|K_d|^2}{E_* \cosh^2(\pi\varepsilon)}\right)^{\frac{1}{2}} \left(\frac{a^2}{\bar{E}_1} g(l/a, \bar{E}_2/\bar{E}_1)\right)^{-\frac{1}{2}}. \tag{21}$$

The minimum stress σ_1 at which steady-state tunneling occurs can be found by equating K_I and $|K_d|$ with the corresponding toughness values K_{Ic} and K_{dc}, respectively, then solving $\partial\sigma_1/\partial l = 0$ for the delamination length l, and subsequently substituting this value back into Eq. (21). As discussed in Suiker and Fleck [20], the delamination at the minimum tunneling stress remains stable.

A straightforward transformation can be used to convert from static loading to fatigue loading at constant amplitude $\Delta\sigma_1$. Consider a fixed rate of fatigue crack growth in the tunneling direction, denoted as da_{tun}/dN. In agreement with Eq. (7), K_I in Eq. (21) may then be replaced by the cyclic stress intensity factor ΔK_I for fatigue crack growth in the material 1 layer at the assumed crack growth rate da_{tun}/dN. As mentioned above, in steady-state tunneling the delamination in the wake of the tunneling crack is not growing (i.e. stable delamination occurs). Thus, the magnitude of the delamination stress intensity $|K_d|$ in Eq. (21) is just below the threshold value ΔK_{dth} for fatigue delamination. Note that the value of $|K_d|$ depends upon the mode-mixity, see Eq. (4); for example, for an H-shape crack in the centre of a relatively thick laminate the delamination is typically in a mode II state [20]. In general, the threshold value ΔK_{dth} may also depend on the

mode-mixity, although in the present study this effect is ignored. It is expected that this does not introduce large errors, since for the delamination problems studied in Suiker and Fleck [20] it was found that the mode-mixity at the delamination tip commonly attains a steady-state value at relatively small delamination lengths. After replacing $|K_d|$ in Eq. (21) by ΔK_{dth}, and rephrasing the expression, the cyclic mode I stress intensity factor becomes

$$\Delta K_I = \sqrt{\frac{\Delta\sigma_1^2 a}{2} g(l/a, \bar{E}_2/\bar{E}_1) - \frac{2l\Delta K_{dth}^2 \bar{E}_1}{aE_* \cosh^2(\pi\varepsilon)}}. \quad (22)$$

Because the cyclic mode I stress intensity factor is real-valued, the term under the square root needs to be non-negative. In the limit of zero delamination ($l = 0$) Eq. (22) reduces to the cyclic stress intensity factor of a tunneling mode I crack, Eq. (14). Substituting Eq. (22) into Eq. (2) provides the growth rate of an H-shape tunneling crack with constant delamination.

2.3. Mechanism 3

Mechanism 3 in Fig. 2c represents an H-shape crack with increasing delamination. The growth of delamination is caused by the fact that the cyclic stress intensity factor for delamination exceeds the threshold value, $\Delta K_d > \Delta K_{dth}$. The elaboration of this mechanism requires 3D simulations in which the transient crack growth in both the tunneling direction, da_{tun}/dN, and along the layer interface, dl/dN, are modelled simultaneously. Such an analysis is beyond the scope of this study. Instead, a simplified case is considered, where the lengthening of the delaminations of the H-shape crack is analysed under *plane-strain conditions*; i.e. the propagation characteristics in the tunneling direction are left out of consideration, see Fig. 3. This case represents the asymptotic limit to which mechanism 3 reduces if the crack length in the tunneling direction becomes infinitely large, and the mode I contribution to the energy dissipation per unit advance of crack tunneling is negligible compared to the contribution by interface delamination [20]. The governing equations for this asymptotic case are presented below.

2.4. Plane-strain H-shape crack with increasing delamination

For the continuously lengthening, plane-strain H-shape crack depicted in Fig. 3 the energy release rate per unit advance of each delamination is

$$G_d = \frac{1}{4}\frac{\partial \Delta W}{\partial l}, \quad (23)$$

with the factor 4 denoting the number of delaminations of the H-shape crack. Combining Eq. (23) with Eqs. (8), (17) and (18) provides the remote stress σ_1 as

$$\sigma_1 = |K_d| \sqrt{\frac{4\bar{E}_1}{aE_* \cosh^2(\pi\varepsilon) g'(l/a, \bar{E}_2/\bar{E}_1)}}, \quad (24)$$

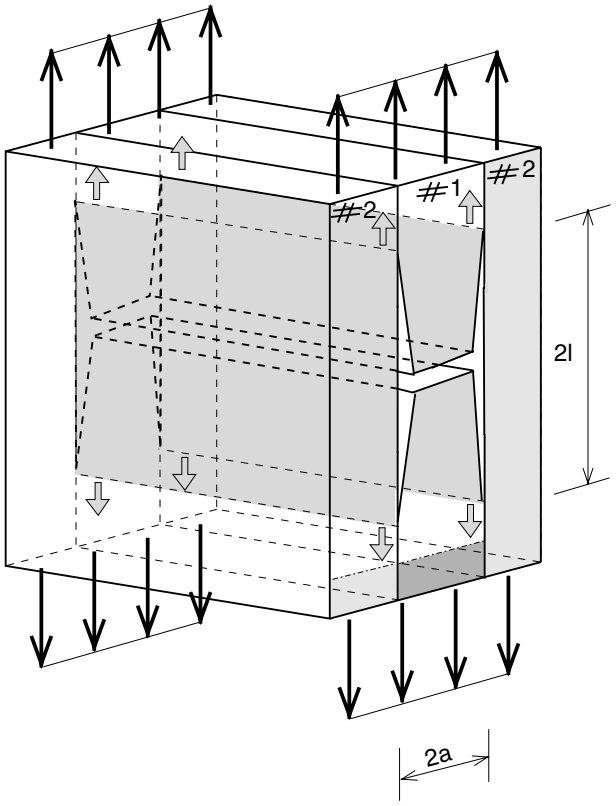

Fig. 3. Plane-strain H-shape crack with continuously increasing delamination.

where g' represents the partial derivative $g' = \partial g/\partial(l/a)$. Equating $|K_d|$with the delamination toughness K_{dc} gives the critical stress for plane-strain delamination. Now consider fatigue delamination by a cyclic stress of amplitude $\Delta\sigma_1$. The cyclic stress intensity factor at the delamination tip follows from Eq. (24) as

$$\Delta K_d = \Delta\sigma_1 \sqrt{\frac{aE_* \cosh^2(\pi\varepsilon)}{4\bar{E}_1} g'(l/a, \bar{E}_2/\bar{E}_1)}. \quad (25)$$

The fatigue delamination growth dl/dN can now be predicted by combining the above expression with the fatigue law, Eq. (6).

3. Fatigue failure mechanism maps for crack tunneling

Calculation of the cyclic stress intensity factor ΔK_I for steady-state crack tunneling with and without delamination requires the determination of the dimensionless functions $g(l/a, \bar{E}_2/\bar{E}_1)$ and $f(\bar{E}_2/\bar{E}_1)$, recall Eqs. (22) and (14). These functions can be derived from 2D finite element analyses, as described by Suiker and Fleck [20] and summarised as follows. From the numerical analyses the displacement profile over the mode I crack faces can be obtained, which, after averaging over the crack width, leads to the average crack opening displacement $\bar{\delta}$. Substituting $\bar{\delta}$ into Eq. (9) gives the function $f(\bar{E}_2/\bar{E}_1)$ characterising the tunneling mode I crack, whereas substituting $\bar{\delta}$ into Eq. (17)

yields the function $g(l/a,\bar{E}_2/\bar{E}_1)$ for a tunneling H-shape crack. In addition, the cyclic stress intensity factor ΔK_d in Eq. (25) for a plane-strain H-shape crack with increasing delamination can be obtained from the numerical computation of the J-integral around the delaminationtip, and combining the equality $G_d = J$ with Eq. (18).

Fig. 4 shows the cross-section of one of the cracked configurations examined in Suiker and Fleck [20]; it is a 5/4 lay-up consisting of 5 layers of material 1 and 4 layers of material 2. The Poisson ratios of materials 1 and 2 are representative for those of many fibre-reinforced laminates, $v_1 = v_2 = 0.3$. The elastic mismatch of the two materials is expressed in terms of the stiffness moduli, $\bar{E}_2/\bar{E}_1$, and the thicknesses of the material 1 and 2 layers are $w_1 = w$ and $w_2 = 5w/6$, respectively. This ratio of ply thicknesses is typical for the fibre–metal laminates ARALL and GLARE, where aluminium sheets of thickness 0.2–0.4 mm are bonded by somewhat thinner fibre–epoxy layers [1,12,18]. The H-shape crack is located in the centre layer (material 1) of the laminate, and has a length $2l$ and a width $2a$. The width of the H-shape crack thus is equal to the thickness of the material 1 layer, $2a = w$. It is assumed that the crack pattern depicted in Fig. 4 has grown from a large pre-existing flaw present in the centre layer, and is driven by a remote fatigue loading characterised by a cyclic tensile strain $\Delta\varepsilon$.

The numerical results for the cracked geometry in Fig. 4 have been reduced to fatigue failure mechanism maps, see Fig. 5. For a tunneling H-shape crack with constant delamination, the curves depicted in Fig. 5b are obtained by inverting Eq. (22) to

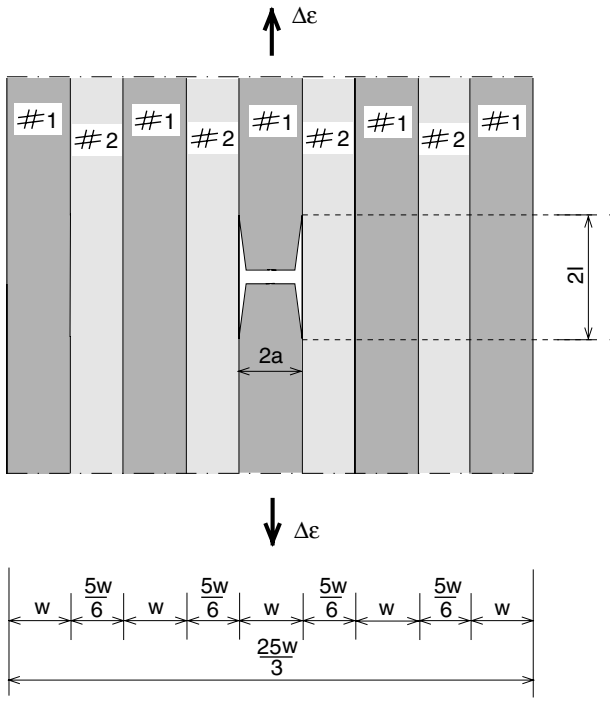

Fig. 4. H-shape cracking in the centre layer of a laminate with a 5/4 lay-up. The remote loading is characterised by a cyclic tensile strain $\Delta\varepsilon$.

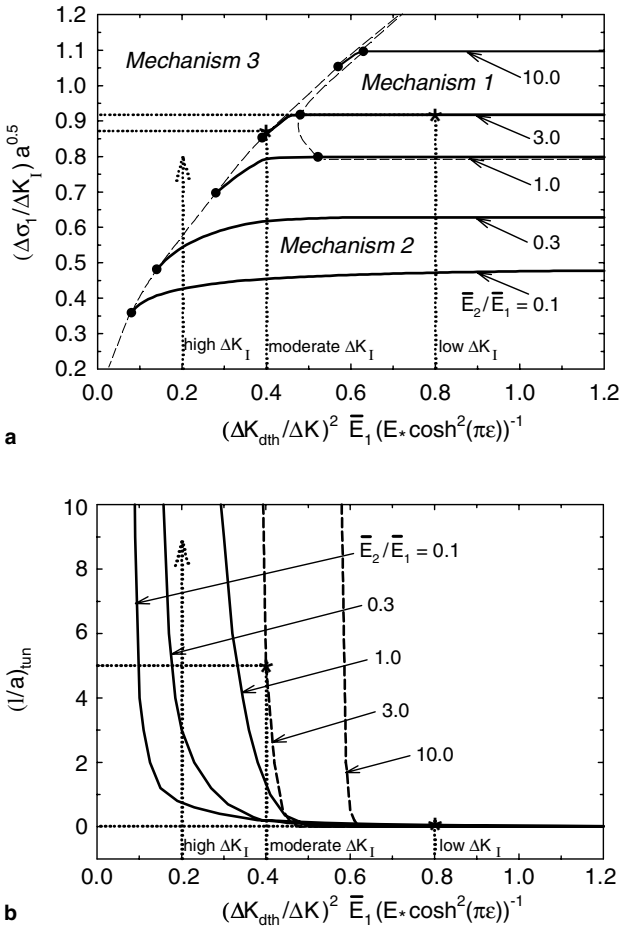

Fig. 5. Fatigue fracture maps for cracking in the centre layer of the 5/4 lay-up, see Fig. 4. (a) Cyclic stress $\Delta\sigma_1$ as a function of the mode I stress intensity factor ΔK_I. Dashed lines indicate the zones corresponding to the three failure mechanisms in Fig. 2. Dotted lines illustrate the interpretation of the figure for three different cyclic stress intensity factors ΔK_I. (b) Tunneling delamination length $(l/a)_{tun}$ as a function of the mode I stress intensity factor ΔK_I. Dotted lines illustrate the interpretation of the figure for three different stress intensity factors ΔK_I.

$$\Delta\sigma_1 = \left(\frac{2aK_I^2}{\bar{E}_1} + \frac{4l\Delta K_{dth}^2}{E_* \cosh^2(\pi\varepsilon)}\right)^{\frac{1}{2}} \left(\frac{a^2}{\bar{E}_1} g(l/a,\bar{E}_2/\bar{E}_1)\right)^{-\frac{1}{2}} \quad (26)$$

and computing, for given ratios $\Delta K_{dth}/\Delta K_I$ and $\bar{E}_2/\bar{E}_1$, the delamination length l for which the above expression for the cyclic stress reaches a *minimum*. At the minimum cyclic stress, Eq. (26) equals the inverted form of Eq. (25), evaluated at the delamination threshold $\Delta K_d = \Delta K_{dth}$, i.e.

$$\Delta\sigma_1 = \Delta K_{dth}\sqrt{\frac{4\bar{E}_1}{aE_* \cosh^2(\pi\varepsilon) g'(l/a,\bar{E}_2/\bar{E}_1)}}. \quad (27)$$

This can be checked by applying the condition $\partial\Delta\sigma_1\partial l = 0$ to Eq. (26), and solving for $\Delta\sigma_1$, which yields Eq. (27). Because the cyclic stress level at which plane-strain delamination is just prohibited, Eq. (27), equals the minimum stress for crack tunneling, Eq. (26), it is assumed that the conditions for a tunneling H-shape crack with constant

delamination (*mechanism 2*) are satisfied. More details on the above procedure can be found in [20]. The minimum cyclic stress is depicted in Fig. 5a as a function of the ratio of stress intensity factors $\Delta K_{\rm dth}/\Delta K_{\rm I}$, at selected stiffness ratios $\bar{E}_2/\bar{E}_1$. For a tunneling mode I crack without delamination ($l=0$), the cyclic stress $\Delta\sigma_1$ plotted in Fig. 5a has been directly obtained from Eq. (14).

In Figs. 5a and b the stress intensity factor $\Delta K_{\rm I}$ acts as the input parameter, and follows from a prescribed crack growth rate through the inversion of the fatigue law, Eq. (2). The three tunneling mechanisms in Fig. 2 are superimposed on Fig. 5a, with the location of their boundaries designated by dashed lines. For each curve of remote cyclic stress versus mode I stress intensity factor the transition from one mechanism to another mechanism is indicated by a black dot. In addition, the dotted lines provide an example of how to use the fracture maps in a fatigue analysis, where, for a chosen stiffness mismatch $\bar{E}_2/\bar{E}_1=3.0$, three possible values of the stress intensity factor $\Delta K_{\rm I}$ are considered. Suppose first that the crack growth rate $da_{\rm tun}/dN$ given by Eq. (2) is relatively low, and relates to a relatively low cyclic stress intensity factor corresponding to $(\Delta K_{\rm dth}/\Delta K_{\rm I})^2\bar{E}_1(E_*\cosh^2(\pi\varepsilon))^{-1}=0.8$. At this value the intersection with the $\Delta\sigma_1-\Delta K_{\rm I}$ curve for $\bar{E}_2/\bar{E}_1=3.0$ (indicated by the asterisk "*") shows that the crack tunnels as a mode I crack (*mechanism 1*) at a remote cyclic stress $\Delta\sigma_1=0.92\Delta K_{\rm I}\ {\rm a}^{-0.5}$. Next, consider a somewhat higher crack growth rate, for which the cyclic stress intensity factor becomes moderately high and relates to $(\Delta K_{\rm dth}/\Delta K_{\rm I})^2\bar{E}_1(E_*\cosh^2(\pi\varepsilon))^{-1}=0.4$. Fig. 5a illustrates that the crack then tunnels as an H-shape crack with constant delamination (*mechanism 2*), in correspondence with a remote cyclic stress $\Delta\sigma_1=0.87\Delta K_{\rm I}\ {\rm a}^{-0.5}$. Finally, if the crack growth rate is relatively high, and relates to a high cyclic stress intensity factor corresponding to $(\Delta K_{\rm dth}/\Delta K_{\rm I})^2\bar{E}_1(E_*\cosh^2(\pi\varepsilon))^{-1}=0.2$. no intersection with the $\Delta\sigma_1-\Delta K_{\rm I}$ curve for $\bar{E}_2/\bar{E}_1=3.0$ is found. This indicates that the crack tunnels as an H-shape crack with continuously increasing delamination (*mechanism 3*); since this mechanism does not reach a steady state, the remote cyclic stress $\Delta\sigma_1$ cannot be obtained from Fig. 5a.

Subsequently, consider the (normalised) delamination length $(l/a)_{\rm tun}$ as a function of the stress intensity factor $\Delta K_{\rm I}$, see Fig. 5b. For $\bar{E}_2/\bar{E}_1=3.0$ and 10.0 it is difficult to obtain the precise shape of the curve in the transition from *mechanism 1* ($(l/a)_{\rm tun}=0$) to *mechanism 3* ($(l/a)_{\rm tun}\to\infty$); this transition occurs abruptly due to the small range of $\Delta K_{\rm I}$ values for which *mechanism 2* is operational, see Fig. 5a. Hence, for $\bar{E}_2/\bar{E}_1=3.0$ and 10.0 the anticipated trends for *mechanism 2* are represented by dashed lines. It can be confirmed that for the low cyclic stress intensity factor related to $(\Delta K_{\rm dth}/\Delta K_{\rm I})^2\bar{E}_1(E_*\cosh^2(\pi\varepsilon))^{-1}=0.8$ *mechanism 1* operates, as characterised by the zero delamination of the tunneling crack. Conversely, *mechanism 2* operates for the moderately high cyclic stress intensity factor related to $(\Delta K_{\rm dth}/\Delta K_{\rm I})^2\bar{E}_1(E_*\cosh^2(\pi\varepsilon))^{-1}=0.4$, with the delamination length of the tunneling crack equal to $(l/a)_{\rm tun}=5$. When the cyclic stress intensity factor is high, in correspondence with $(\Delta K_{\rm dth}/\Delta K_{\rm I})^2\bar{E}_1(E_*\cosh^2(\pi\varepsilon))^{-1}=0.2$, *mechanism 3* is active: the delamination length continuously grows.

Tunneling fatigue cracks without delamination (*mechanism 1*) have been observed experimentally in glass-fibre reinforced plastic laminates [28,29]. From the results depicted in Fig. 5, it may be concluded that for these materials the interfaces between the fibres and the matrix are relatively strong, such that the fatigue threshold value $\Delta K_{\rm dth}$ is sufficiently high to prevent interfacial delamination. In contrast, for the fibre–metal laminates ARALL and GLARE, there is ample experimental evidence of tunneling H-shape cracks (*mechanisms 2* and *3*) developing in centre-cracked specimens subjected to cyclic loading [1,2,12,14,15,18]. H-shape cracks have also been observed in the fatigue crack tunneling of fibrous composites, such as 0/90 cross-ply carbon fibre–epoxy matrix laminates [5] and fibre-reinforced titanium alloys [4,16,19]. For these materials the interfacial fatigue threshold $\Delta K_{\rm dth}$ is sufficiently low for delamination to occur.

Fig. 5a illustrates the transition in fracture scenarios from *mechanism 1* to *mechanism 2*, and subsequently to *mechanism 3*, when the cyclic mode I stress intensity factor $\Delta K_{\rm I}$ increases from a 'low' value to a 'moderate' value, and finally to a 'high' value. A higher cyclic stress level thus induces more delamination, a phenomenon that is commonly observed experimentally for tunneling H-shape cracks in fibre-reinforced composites and fibre–metal laminates [1,2,5,18]. Fatigue tests on centre-cracked GLARE specimens performed by Takamatsu et al. [12] indicated clearly that at a moderate gross cyclic stress level of 110 MPa the delamination as well as the tunneling crack growth rate of the H-shape crack after some tunneling distance become constant (*mechanism 2*), whereas at higher cyclic stress levels of 147 and 196 MPa the delamination and the tunneling crack growth rate continuously increase with tunneling distance (*mechanism 3*). This transition in failure mechanisms is predicted by the present model, see Fig. 5a. Although the laminates tested by Takamatsu et al. [12] have the same lay-up as the configuration depicted in Fig. 4, their test data may not be quantitatively compared to the present model, since in the experiments crack tunneling was observed in *all* metal layers whereas in the model crack tunneling only occurs in the centre metal layer.

It is worth mentioning that *mechanism 2* is hard to observe if the laminate thickness becomes small. Numerical simulations in Suiker and Fleck [20] showed that for a 2/1 lay-up the lateral stiffness of the laminate is too low for adequately supporting stable delamination with a measurable and constant delamination length. Translating the virtual absence of *mechanism 2* for thin laminates towards the case of fatigue fracture means that a continuous increase of the cyclic mode I stress intensity factor $\Delta K_{\rm I}$ at a certain point will induce an abrupt transition from *mechanism 1* to *mechanism 3*. The absence of *mechanism 2* for very thin laminates seems to be confirmed by the experiments of Guo

and Wu [13], where for a centre-cracked tensile specimen of GLARE with a 2/1 lay-up subjected to a moderate cyclic stress level of 120 MPa the tunneling crack developed delamination but the tunneling crack growth rate did not reach a constant (steady-state) value. This implies that crack tunneling occurs through *mechanism 3*. In contrast, for a thicker 3/2 lay-up the tunneling cracks driven by cyclic stress levels of 120 and 150 MPa in both cases developed delamination and did reach a steady state. This suggests that in the thicker 3/2 lay-up *mechanism 2* is activated at moderate cyclic stress levels.

4. Analytical expression for steady-state plane-strain delamination

In this section, the lengthening of the delaminations of an H-shape crack under *plane-strain conditions* is considered. The cyclic stress intensity factor at the delamination tip ΔK_{d} is given by Eq. (25), and can be determined from the numerical computation of the J-integral around the delamination tip, see [20]. The lay-ups analysed numerically in Suiker and Fleck [20] showed that for delaminations exceeding a few times the layer thickness the stress intensity factor ΔK_{d} given by Eq. (25) closely approaches the asymptotic steady-state value $\Delta K_{\mathrm{d,ss}}$ for infinite delamination, $l/a \to \infty$. The steady-state cyclic stress intensity factor $\Delta K_{\mathrm{d,ss}}$ can be computed in closed form by considering the energy balance with respect to cross-sections downstream and upstream of the delamination tip (see also, [24]). Expressions for $\Delta K_{\mathrm{d,ss}}$ are derived for an $n/(n-1)$ laminate, with the notation "$n/(n-1)$" referring to a laminate of n layers of material 1 alternately stacked with $n-1$ layers of material 2. The crack patterns considered are an H-shape crack in the centre layer of the laminate, see Fig. 6a, and a doubly-deflected crack in the two outer layers of the laminate, see Fig. 6b. Notice that the doubly deflected cracks in the two outer layers taken together construct an H-shape crack of width $4a$. Under an external loading P, the upstream cross-section of these laminates should meet the equilibrium requirement

$$\sigma_1 t_1 + \sigma_2 t_2 = P, \tag{28}$$

where t_1 and t_2 are the total upstream cross-sections of materials 1 and 2, respectively. Similarly, equilibrium at the downstream cross-section (i.e. at the mid-plane) is defined by

$$\sigma_1^{\mathrm{m}} t_1^{\mathrm{m}} + \sigma_2^{\mathrm{m}} t_2^{\mathrm{m}} = P, \tag{29}$$

with σ_1^{m} and σ_2^{m} the downstream stresses, and t_1^{m} and t_2^{m} the total downstream cross-sections of materials 1 and 2, respectively. Equating Eqs. (28) and (29), and combining the result with the compatibility statements

$$\frac{\sigma_1}{\bar{E}_1} = \frac{\sigma_2}{\bar{E}_2} \quad \text{and} \quad \frac{\sigma_1^{\mathrm{m}}}{\bar{E}_1} = \frac{\sigma_2^{\mathrm{m}}}{\bar{E}_2}, \tag{30}$$

leads to

$$\sigma_2^{\mathrm{m}} = \sigma_1 \frac{\bar{E}_2}{\bar{E}_1} \left(\frac{\bar{E}_1 t_1 + \bar{E}_2 t_2}{\bar{E}_1 t_1^{\mathrm{m}} + \bar{E}_2 t_2^{\mathrm{m}}} \right). \tag{31}$$

The energy consumed during delamination, ΔW, equals the difference in strain energy downstream and upstream of the delamination tip,

$$\Delta W = l \left(\frac{t_1^{\mathrm{m}} (\sigma_1^{\mathrm{m}})^2 - t_1 \sigma_1^2}{2\bar{E}_1} + \frac{t_2^{\mathrm{m}} (\sigma_2^{\mathrm{m}})^2 - t_2 \sigma_2^2}{2\bar{E}_2} \right). \tag{32}$$

By taking the derivative of ΔW with respect to the delamination length l, and combining the result with Eqs. (30) and (31), the steady-state (plane-strain) energy release rate per unit advance of delamination is obtained as

$$\begin{aligned} G_{\mathrm{d,ss}}^{*} &= \frac{\partial \Delta W}{\partial l} \\ &= \frac{\sigma_1^2 (t_1 \bar{E}_1 + t_2 \bar{E}_2)(\bar{E}_1 (t_1 - t_1^{\mathrm{m}}) + \bar{E}_2 (t_2 - t_2^{\mathrm{m}}))}{2\bar{E}_1^2 (t_1^{\mathrm{m}} \bar{E}_1 + t_2^{\mathrm{m}} \bar{E}_2)}. \end{aligned} \tag{33}$$

The total steady-state energy release rate, $G_{\mathrm{d,ss}}^{*}$, reduces to the steady-state energy release rate per delamination, $G_{\mathrm{d,ss}}$, upon dividing $G_{\mathrm{d,ss}}^{*}$ by the number of delamination tips j,

$$G_{\mathrm{d,ss}} = \frac{G_{\mathrm{d,ss}}^{*}}{j}. \tag{34}$$

For an H-shape crack in the centre of the $n/(n-1)$ laminate (Fig. 6a) the total energy release rate at the delamination tips can be computed through substituting

$$t_1 = n w_1, \qquad t_1^{\mathrm{m}} = (n-1) w_1, \qquad t_2 = t_2^{\mathrm{m}} = (n-1) w_2, \tag{35}$$

into Eq. (33) and subsequently inserting the result into Eq. (34), with the number of delamination tips as $j = 2$ (only half of the geometry is considered, see Fig. 6). This leads to

$$G_{\mathrm{d,ss}} = \frac{\sigma_1^2}{4\bar{E}_1} \left(\frac{w_1 (n w_1 \bar{E}_1 + (n-1) w_2 \bar{E}_2)}{(n-1)(w_1 \bar{E}_1 + w_2 \bar{E}_2)} \right). \tag{36}$$

Similar asymptotic solutions can be found in other works [1,30,20]. Employing Eq. (18), Eq. (36) can be rephrased as

$$\sigma_1 = \mid K_{\mathrm{d,ss}} \mid \sqrt{\frac{4\bar{E}_1}{w_1 E_* \cosh^2(\pi\varepsilon)} \frac{(n-1)(w_1 \bar{E}_1 + w_2 \bar{E}_2)}{(n w_1 \bar{E}_1 + (n-1) w_2 \bar{E}_2)}}. \tag{37}$$

Now, specifying Eq. (37) to fatigue loading provides the cyclic stress intensity factor under steady-state conditions as

$$\begin{aligned} \Delta K_{\mathrm{d,ss}} &= \Delta\sigma_1 \\ &\quad \times \sqrt{\frac{w_1 E_* \cosh^2(\pi\varepsilon)}{4\bar{E}_1} \frac{(n w_1 \bar{E}_1 + (n-1) w_2 \bar{E}_2)}{(n-1)(w_1 \bar{E}_1 + w_2 \bar{E}_2)}}. \end{aligned} \tag{38}$$

Note that the above relation agrees with the general expression, Eq. (25). Inserting Eq. (38) into Eq. (6) gives the fatigue delamination rate for an H-shape crack in the centre layer of an $n/(n-1)$ laminate.

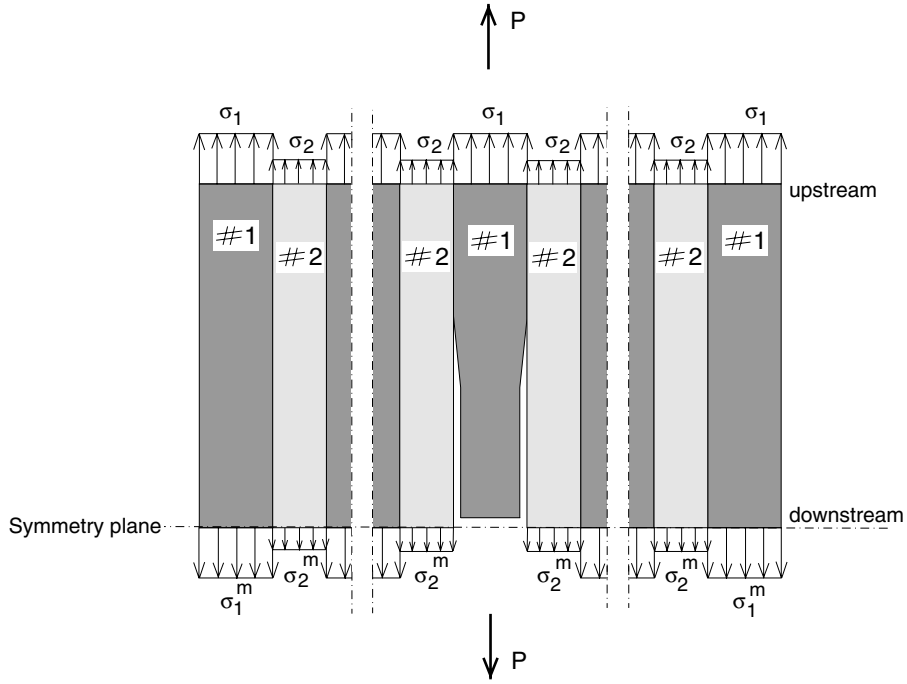

a) H-shape in centre layer of laminate

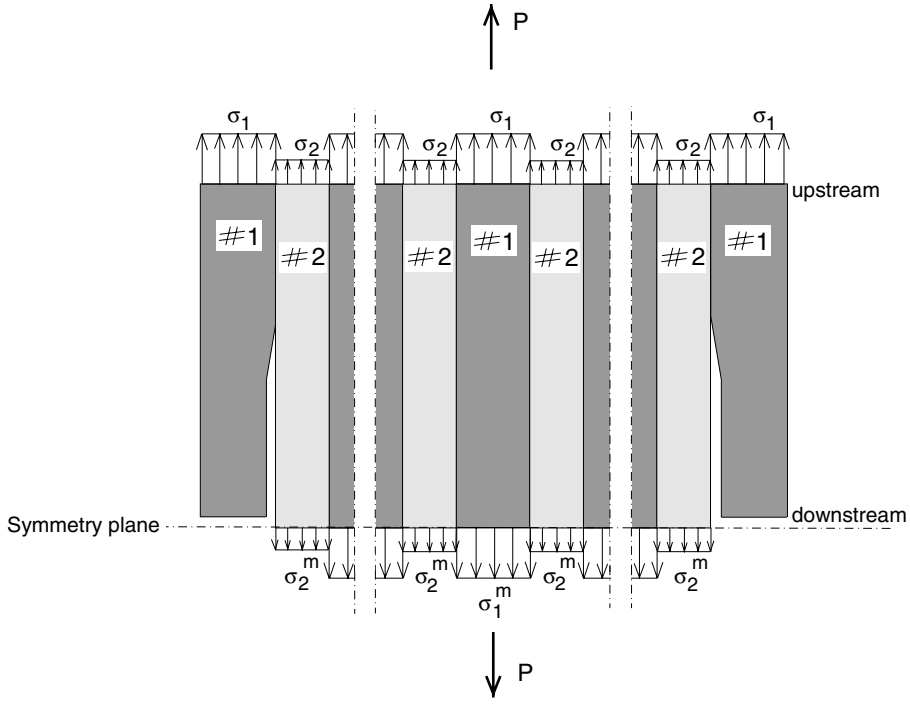

b) Doubly-deflected crack in two outer layers of laminate

Fig. 6. Laminate subjected to plane-strain delamination. The force P denotes the equilibrium between "upstream" and "downstream" cross-sections. (a) H-shape crack in the centre layer of the laminate, (b) doubly-deflected crack in the two outer layers of the laminate.

Subsequently, a doubly-deflected crack in the two outer layers of an $n/(n-1)$ laminate (Fig. 6b) is specified through

$$t_1 = nw_1, \quad t_1^{\mathrm{m}} = (n-2)w_1, \quad t_2 = t_2^{\mathrm{m}} = (n-1)w_2. \tag{39}$$

Using a similar derivation procedure as outlined above, the steady-state cyclic stress intensity factor is

$$\Delta K_{\mathrm{d,ss}} = \Delta\sigma_1 \sqrt{\frac{w_1 E_* \cosh^2(\pi\varepsilon)}{4\bar{E}_1} \frac{2(nw_1\bar{E}_1 + (n-1)w_2\bar{E}_2)}{((n-2)w_1\bar{E}_1 + (n-1)w_2\bar{E}_2)}}. \tag{40}$$

Inserting Eq. (40) into Eq. (6) provides the delamination growth rate.

The fatigue fracture maps depicted in Fig. 5 and the closed-form expressions Eqs. (38) and (40) are useful in the prediction of the delamination growth rates of fibre–metal laminates. However, they should be treated with care when fatigue failure is dominated by effects that have not been taken into account in the model, such as the presence of significant residual stresses in the layers, substantial yielding in the metal layers, or breakage and pull-out of fibres.

5. Comparison with fatigue experiments

The delamination fatigue model presented above is now validated to test data of constant amplitude fatigue experiments on ARALL panels, as reported by Marissen [1]. In these experiments the delamination growth rate $\mathrm{d}l/\mathrm{d}N$ of a 2/1 lay-up was measured under various cyclic stress levels $\Delta\sigma_1$. The effect of the lay-up geometry on the delamination growth rate was studied by testing laminates with various ply thicknesses w_1 and w_2. The loading frequency in the fatigue tests ranged between 5 and 30 Hz; at higher load levels the frequency was taken lower in order to avoid excessive heating of the specimen. The specimen length and width were equal to $L = 300$ mm, $W = 20$ mm, respectively. The aluminium layers were pre-cracked over the full specimen width, see Fig. 7. Accordingly, the fracture energy released during an external cyclic loading ΔP may be completely ascribed to delamination. The delamination growth rate was measured when the delamination reached a value of $l \approx 10$ mm, which, depending on the thickness of the aluminium layer w_1, relates to normalised delaminations in the range of $10 < l/w_1 < 36$. As demonstrated in Suiker and Fleck [20], the growth characteristics for such delaminations closely approach those of the asymptotic case with infinite delamination. Hence, it is expected that the steady-state delamination growth rate can be closely approximated through Eqs. (6) and (40). The delamination was measured by means of a photo-elastic technique. The aramid fibres were oriented in the loading direction of the specimen, where the stiffness of the fibre–epoxy layers in the loading direction was $E_2 = 48.6$ GPa. The stiffness of the aluminium layers was $E_1 = 72$ GPa, and both the aluminium and fibre–epoxy layers had a Poisson's ratio of 0.33. Combining these stiffness values with Eqs. (19) and (20) provides the oscillatory index of the bi-material as $\varepsilon = -0.016$. The load ratio R, defined as the ratio between the minimum and maximum gross stresses measured during a cycle, was relatively low, $R = 0.05$ (i.e. close to the the load ratio for fully reversed loading, $R = 0$). Furthermore, the tensile residual stresses generated in the aluminium layer during manufacturing were small (less than 25 MPa).

In Fig. 8 the experimental data of Marissen [1] are depicted together with the predictions of Eqs. (6) and (40), with the scaling constants taken as $B = 4.8 \times 10^{-12}$ m/cycle $\cdot$ $(\mathrm{MPa}\sqrt{s})^{-s}$ and $s = 8.23$, and the number of

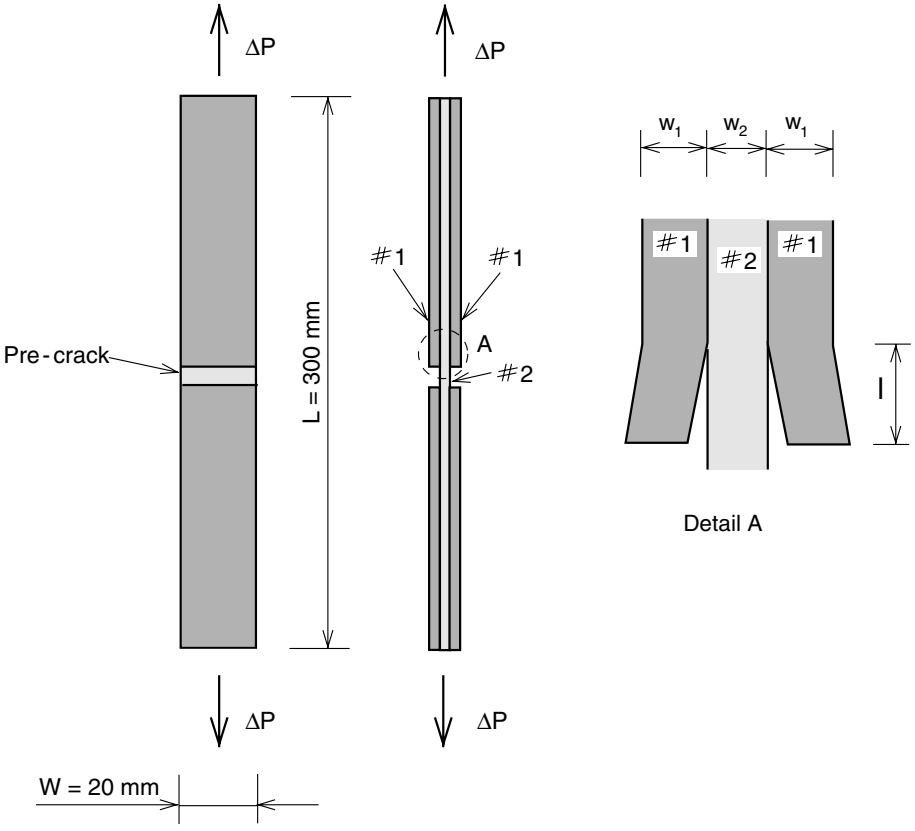

Fig. 7. ARALL 2/1 lay-up with a pre-crack half way the specimen length that is subjected to an external cyclic loading ΔP.

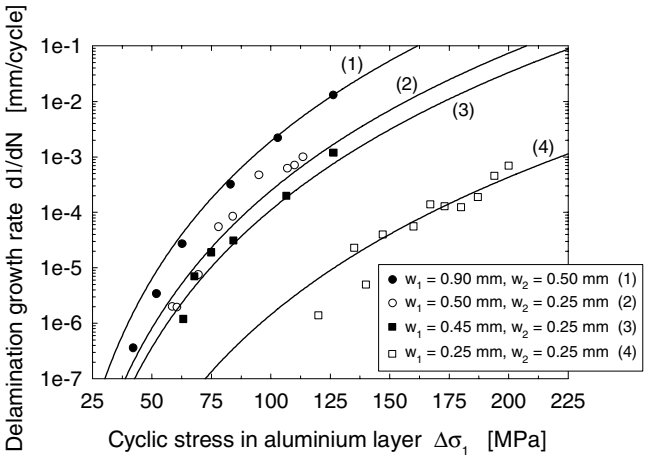

Fig. 8. Delamination growth rate dl/dN versus remote cyclic stress in aluminium layer $\Delta\sigma_1$ for ARALL 2/1 lay-ups (see Fig. 7) with various ply thicknesses w_1 and w_2. Experiments (symbols) versus model (solid lines). The experimental values are taken from Marissen [1]. The model results are computed using Eqs. (6) and (40), with $s = 8.23$ and $B = 4.8 \times 10^{-12}$ m/cycle·$(\mathrm{MPa}\sqrt{s})^{-s}$.

aluminium layers equal to $n = 2$. For all lay-ups the fatigue model is in excellent agreement with the experimental results. Both the experimental results and the fatigue model illustrate that an increasing thickness of the aluminium layers leads to a higher delamination growth rate. This is because the aluminium is relatively stiff, and an increase of the aluminium plate thickness increases the cyclic stress intensity at the delamination tip, and thus the delamination growth rate.

6. Concluding remarks

Fracture mechanics solutions of a recent study on crack tunneling in laminates have been combined with a Paris-type fatigue law to simulate the crack growth rate under constant amplitude fatigue loading. Depending on the applied cyclic stress level three possible mechanisms can develop, which differ by the amount of delamination generated. The actual fracture mechanism that is activated strongly depends on the ratio between the delamination fatigue threshold and the cyclic stress intensity factor at the tunneling mode I crack tip, $\Delta K_{\mathrm{dth}}/\Delta K_{\mathrm{I}}$. It has been shown that the fatigue crack growth rate of steady-state tunneling cracks can be predicted by using fracture maps constructed from 2D numerical analyses. The present model loses its validity when the steady-state propagation of the tunneling crack is disturbed. This may occur when the tunneling crack encounters imperfections within a layer or at a layer interface, or when a panel boundary is reached. Furthermore, steady-state propagation conditions will not be reached if the cyclic stress intensity factor at the tunneling crack front becomes relatively high, where an H-shape crack with constant delamination converts into an H-shape crack with continuously growing delamination. In addition to the simulation of tunneling cracks, a fatigue model for a plane-strain H-shape crack with continuously increasing delamination has been formulated. By means of a comparison with experimental data taken from the literature it has been demonstrated that the model provides accurate predictions of the delamination growth rate for various lay-ups.

Acknowledgements

Both authors are grateful for the support provided by the European Community's Human Potential Program, contract HPRN-CT-2002-00198, (DEFINO). A.S.J.S. is grateful for the hospitality offered by the Cambridge Centre for Micromechanics at the Cambridge University, Cambridge, United Kingdom, during an 8 month leave from the Delft University of Technology, Delft, The Netherlands.

References

[1] Marissen R. Fatigue crack growth in ARALL – a hybrid aluminium–aramid composite material. Ph.D. Thesis. Delft University of Technology, The Netherlands; 1988.
[2] Ritchie RO, Yu W, Bucci RJ. Fatigue crack propagation in ARALL laminates: measurement of the effect of crack-tip shielding from crack bridging. Eng Frac Mech 1989;32:361–77.
[3] Evans AG, He MY, Hutchinson JW. Interface debonding and fiber cracking in brittle matrix composites. J Am Ceram Soc 1989;72:2300–3.
[4] Cox BN, Marshall DB. Crack bridging in the fatigue of fibrous composites. Fatigue Fract Eng Mater Struct 1991;14:847–61.
[5] Spearing SM, Beaumont PWR. Fatigue damage mechanics of composite materials. I. Experimental measurement of damage and post-fatigue properties. Comp Sci Technol 1992;44:159–68.
[6] Cox BN, Marshall DB. Overview no. 111, concepts for bridged cracks in fracture and fatigue. Acta Metall Mater 1994;42:341–63.
[7] Cox BN, Rose LRF. Time- or cycle-dependent crack bridging. Mech Mater 1994;19:39–57.
[8] Folsom CA, Zok FW, Lange FF. On the flexural properties of brittle multilayer materials. I. Modeling. J Am Ceram Soc 1994;77:689–96.
[9] Folsom CA, Zok FW, Lange FF. On the flexural properties of brittle multilayer materials. II. Experiments. J Am Ceram Soc 1994;77:2081–7.
[10] Boniface L, Smith PA, Bader MG, Rezaifard AH. Transverse ply cracking in cross-ply CFRP laminates – initiation or propagation controlled? J Compos Mater 1996;31:1080–112.
[11] Lin CT, Kao PW. Delamination growth and its effect on crack propagation in carbon fiber reinforced aluminium laminates under fatigue loading. Acta Mater 1996;44:1181–8.
[12] Takamatsu T, Matsumura T, Ogura N, Shimokawa T, Kakatu Y. Fatigue crack growth properties of a GLARE-3-5/4 fiber/metal laminate. Eng Fract Mech 1999;63:253–72.
[13] Guo Y-J, Wu X-R. A theoretical model for predicting fatigue crack growth rates in fibre-reinforced metal laminates. Fatigue Fract Eng Mater Struct 1998;21:1133–45.
[14] Guo Y-J, Wu X-R. A phenomenological model for predicting crack growth in fibre-reinforced metal laminates under constant-amplitude loading. Compos Sci Technol 1999;59:1825–31.
[15] Vlot A, Gunnink JW, editors. Fibre metal laminates – an introduction. Dordrecht: Kluwer Academic Publishers; 2001.
[16] Rhymer DW, Johnson WS. Fatigue damage mechanisms in advanced hybrid titanium composite laminates. Int J Fatigue 2002;24:995–1001.

[17] Burianek DA, Spearing SM. Modeling of facesheet crack growth in titaniumgraphite hybrid materials. Part II. Experimental results. Eng Frac Mech 2003;70:799–812.
[18] Shim DJ, Alderliesten RC, Spearing SM, Burianek DA. Fatigue crack growth in GLARE hybrid laminates. Compos Sci Technol 2003;63:1759–67.
[19] Cortes P, Cantwell WJ. The tensile and fatigue properties of carbon fibre-reinforced peek-titanium fibre–metal laminates. J Reinf Plast Compos 2004;23:1615–23.
[20] Suiker ASJ, Fleck NA. Crack tunneling and plane-strain delamination in layered solids. Int J Frac 2004;125:1–32.
[21] Paris PC, Gomez MP, Anderson WP. A rational analytic theory of fatigue. Trend Eng 1961;13:9–14.
[22] Hutchinson JW, Mear M, Rice J. Crack paralleling an interface between dissimilar materials. J Appl Mech (ASME) 1987;54:828–32.
[23] Rice JR. Elastic fracture concepts for interfacial cracks. J Appl Mech (ASME) 1988;55:98–103.
[24] Hutchinson JW, Suo Z. Mixed mode cracking in layered materials. Adv Appl Mech 1992;29:63–191.
[25] Beuth JL. Cracking of thin bonded films in residual tension. Int J Solids Struct 1992;29:1657–75.
[26] Ho S, Suo Z. Tunneling cracks in constrained layers. J Appl Mech (ASME) 1993;60:890–4.
[27] Dundurs J. Edge-bonded dissimilar orthogonal elastic wedges. J Appl Mech (ASME) 1969;36:650–2.
[28] Ogin SL, Smith PA. Fast fracture and fatigue growth of transverse ply cracks in composite laminates. Scripta Metall 1985; 19:779–84.
[29] Tong J, Guild FJ, Ogin SL, Smith PA. On matrix crack growth in quasi-isotropic laminates. I. Experimental investigation. Comp Sci Technol 1997;57:1527–35.
[30] Burianek DA, Spearing SM. Delamination growth from face sheet seams in cross-ply titanium/graphite hybrid laminates. Compos Sci Technol 2001;61:261–9.